

## SUPPORTING INFORMATION

### Synthesis of faceted $\beta$ -SnWO<sub>4</sub> microcrystals with enhanced visible-light photocatalytic properties

Jan Ungelenk and Claus Feldmann\*

Karlsruhe Institute of Technology (KIT), Institute of Inorganic Chemistry, Engesserstraße 15, D-76131 Karlsruhe, Germany.

E-mail: claus.feldmann@kit.edu

Fax: +49 (0)721 608-44892, Tel: +49 (0)721 608-42856

#### 1. Analytical tools for characterization:

Scanning electron microscopy (SEM) was carried out with a Zeiss Supra 40 VP microscope. Diluted aqueous or ethanolic suspensions of as-prepared products were deposited on silicon wafers and evaporated in vacuum. The acceleration voltage was in the range of 5–10 kV and the working distance was 3 mm. Energy-dispersive X-ray analysis (EDX) was carried out using an AMETEC EDAX mounted on the above described SEM using spot-EDX on single faceted  $\beta$ -SnWO<sub>4</sub> microcrystals. X-ray powder diffraction (XRD) was performed with a Stoe STADI-P diffractometer operating with Ge-monochromatized Cu-K $\alpha$ -radiation ( $\lambda = 1.54178 \text{ \AA}$ ). Sorption measurements were performed based on Brunauer-Emmett-Teller (BET) analysis. To this concern, as-prepared powder samples were measured with a BELSORPmini II from BEL, applying N<sub>2</sub> as adsorbate. Fourier-transformed infrared (FT-IR) spectra were recorded with a Bruker Vertex 70 FT-IR spectrometer; the samples were measured as pellets in KBr with a resolution of 4 cm<sup>-1</sup>. Diffuse reflectance spectra of powders were recorded in a wavelength interval of 250–800 nm with a Varian Cary 100 spectrometer, equipped with an integrating sphere against BaSO<sub>4</sub> as a reference.

#### 2. Experimental details and sample preparation

**Chemicals:** Tin dichloride (SnCl<sub>2</sub>, ABCR), sodium tungstate dihydrate (Na<sub>2</sub>WO<sub>4</sub>·2H<sub>2</sub>O, Riedel-de-Haën), bismuth nitrate pentahydrate (Bi(NO<sub>3</sub>)<sub>3</sub>·5H<sub>2</sub>O, Riedel-de-Haën), ammonium metavanadate (NH<sub>4</sub>VO<sub>3</sub>, Riedel-de-Haën), sodium metavanadate (NaVO<sub>3</sub>, Riedel-de-Haën), silver nitrate (AgNO<sub>3</sub>, Riedel-de-Haën), disodium hydrogen orthophosphate dodecahydrate (Na<sub>2</sub>HPO<sub>4</sub>·12H<sub>2</sub>O, Merck), disodium hydrogen orthophosphate dihydrate (Na<sub>2</sub>HPO<sub>4</sub>·2H<sub>2</sub>O, Merck), cetyltrimethylammonium bromide (CTAB, (C<sub>16</sub>H<sub>33</sub>)N(CH<sub>3</sub>)<sub>3</sub>Br, ABCR), *n*-dodecan (C<sub>12</sub>H<sub>26</sub>, ABCR), diethylene glycol (DEG, (HOCH<sub>2</sub>CH<sub>2</sub>)<sub>2</sub>O, Sigma-Aldrich), *n*-hexanol (C<sub>6</sub>H<sub>13</sub>OH,

Fluka), absolute ethanol (Seulberger), methanol (Fluka), nitric acid 65 wt-% (VWR), sodium hydroxide (VWR), urea ( $\text{CO}(\text{NH}_2)_2$ , ABCR), hydrazine solution 35 wt-% in  $\text{H}_2\text{O}$  ( $\text{N}_2\text{H}_4$  (aq), Sigma-Aldrich), hydrochloric acid (Seulberger), bismuth vanadate ( $\text{BiVO}_4$ , Alfa-Aesar), Degussa P25 ( $\text{TiO}_2$ , Degussa), deionized water. All reagents used were analytically pure and were used without further purification.

**Preparation of faceted  $\beta\text{-SnWO}_4$  microcrystals (title-compound, sample i):** In a typical synthesis, a w/o- (water-in-oil)-microemulsion consisting of 25.0 mL of n-dodecane as the non-polar phase, 0.910 g (2.5 mmol) of CTAB as the surfactant and 2.5 mL of *n*-hexanol as the co-surfactant were established under continuous nitrogen flow. After heating to 60 °C, the mixture was loaded with 1 mL of a 0.6 M methanolic solution of  $\text{SnCl}_2$  (0.114 g) as the polar phase. As a result, a clear, homogenous reverse microemulsion is formed. Under vigorous stirring 1 mL of an equimolar aqueous solution of  $\text{Na}_2\text{WO}_4 \cdot 2\text{H}_2\text{O}$  (0.198 g) was added and led to an immediate formation of a yellow suspension, due to nucleation of  $\beta\text{-SnWO}_4$ . Thereafter, the temperature was raised to 200 °C within 15 min and maintained for one hour, while volatile components were distilled off. Finally, the reaction was quenched by addition of 20 mL of DEG to the hot reaction mixture. The microcrystals accumulated at the phase boundary and were collected by centrifugation, after naturally cooling to room temperature. The obtained solid was washed with diluted hydrazinium dichloride solution to remove remaining surfactant from the particle surface. Finally, the faceted  $\beta\text{-SnWO}_4$  microcrystals were washed several times via sequential resuspension/centrifugation in/from ethanol. In the course of this multistep washing procedure, part of the product is lost. Therefore, an approximate final yield of 50–60% of faceted  $\beta\text{-SnWO}_4$  microcrystals was obtained. Finally, the solid was dried in vacuum at room temperature.

**Preparation of X-ray amorphous nanoscaled  $\beta\text{-SnWO}_4$  (sample h):** Nanoscaled  $\beta\text{-SnWO}_4$  was synthesized by precipitation utilizing electrostatic stabilization. In a typical recipe,  $\text{SnCl}_2$  (417.1 mg, 2.2 mmol) was dissolved in 2.5 mL of deionized water. Under vigorous magnetic stirring, this solution was added to 2.5 mL of an equimolar aqueous solution of  $\text{Na}_2\text{WO}_4 \cdot 2\text{H}_2\text{O}$  (725.7 mg) at ambient temperature. A bright yellow nanomaterial was generated and the resulting suspension was directly diluted with 20 mL of deionized water. The obtained nanomaterial was collected by centrifugation (15 min, 25.000 rpm), redispersed two times in deionized  $\text{H}_2\text{O}$  and centrifuged again for washing. Powder material was obtained by centrifugation and drying in air at 60 °C. Subsequently, the powder was dried in vacuum at room temperature in order to remove remaining volatiles. Optionally, larger particles and agglomerates were removed by centrifugation.

**Preparation of bulk- $\beta\text{-SnWO}_4$  (sample c, Jeitschko-synthesis):** Bulk- $\beta\text{-SnWO}_4$  was prepared after the established solid state reaction, followed by rapid thermal quenching originally reported by Jeitschko and Sleight.<sup>[1]</sup> Thoroughly pestled equimolar mixtures of  $\text{SnO}$  and  $\text{WO}_3$  were heated under argon atmosphere in a silica tube, equipped with a pressure-relief valve, to 800 °C. After soaking for 2 h in argon atmosphere, the mixture was first slowly cooled to 700 °C and then rapidly quenched in ice water.

**Preparation of  $m$ -BiVO<sub>4</sub> microcrystals (sample d, Kudo-synthesis):** A slightly modified route as originally described by Kudo *et al.* was used to synthesize faceted  $m$ -BiVO<sub>4</sub> microcrystals.<sup>[2]</sup> 6.4 mmol (3.104 g) of Bi(NO<sub>3</sub>)<sub>3</sub>·5H<sub>2</sub>O were suspended in 16 mL deionized water. An equimolar amount (0.749 g) of NH<sub>4</sub>VO<sub>3</sub> was dissolved in 16 mL of 1.6 M HNO<sub>3</sub> and added to this first solution. Afterwards, 20 mmol of urea (1.201 g) were added. The resulting suspension was stirred at 90 °C for 8 h. The solid was washed several times by sequential resuspension/centrifugation in/from deionized water and dried in vacuum at room temperature.

**Preparation of faceted Ag<sub>3</sub>PO<sub>4</sub> rhombic dodecahedrons (sample g, Je-synthesis):** Faceted Ag<sub>3</sub>PO<sub>4</sub> microcrystals of rhombic dodecahedral shape were reproduced from a published precipitation route.<sup>[3]</sup> In a typical synthesis, freshly prepared and washed silver acetate 1.12 mmol (187 mg, prepared from dissolution of freshly precipitated silver carbonate in acetic acid at 60 °C in the dark) was solved in 20 mL of distilled water in the dark – like most silver compounds, silver acetate is light-sensitive. To this clear solution 2.5 mL of a 0.15 M aqueous solution of Na<sub>2</sub>HPO<sub>4</sub> · 2H<sub>2</sub>O (66.8 mg, 0.375 mmol) were added drop by drop in the dark, whereupon a bright yellow product slowly precipitated. The obtained suspensions were centrifuged (15 min, 25.000 rpm) and redispersed two times in deionized H<sub>2</sub>O for washing. Powder material was obtained by centrifugation and drying in air in the dark.

**Preparation of bulk-Ag<sub>3</sub>PO<sub>4</sub> (sample f, Je-synthesis):** Another bulk-Ag<sub>3</sub>PO<sub>4</sub> benchmark photocatalyst was prepared by a simple ion-exchange method reported in the literature.<sup>[4]</sup> Raw powders of Na<sub>2</sub>HPO<sub>4</sub>·12H<sub>2</sub>O (2.0 mmol, 358.1 mg) and AgNO<sub>3</sub> (6.0 mmol, 1.019 g) were well pestled resulting in a color change to yellow indicating the formation of Ag<sub>3</sub>PO<sub>4</sub>. The powder was washed several times by sequential resuspension/centrifugation in/from deionized water and dried in air in the dark.

The commercial samples in the following are denoted as sample **b** (BiVO<sub>4</sub>, Alfa-Aesar) and sample **e** (TiO<sub>2</sub>, Degussa P25).

### 3. Sample preparation and continuative sample characterization

In addition to X-ray powder diffraction analysis (*cf.* Fig 1 of the main manuscript), the chemical composition of the faceted  $\beta$ -SnWO<sub>4</sub> microcrystals (title compound, sample **i**) was validated by EDX analysis (Figure S1). Accordingly, spot-EDX analysis of single faceted microcrystals confirmed the stoichiometry with a Sn : W ratio of 0.99 : 1 (calculated 1 : 1). As a low-weight element, oxygen cannot be quantified by EDX with the required significance. Note also that only Sn, W and O were detected. Potential impurities such as sodium or halides – eventually remaining from the starting materials – were not detected by EDX analysis, indicating a successful washing procedure and a pure sample.

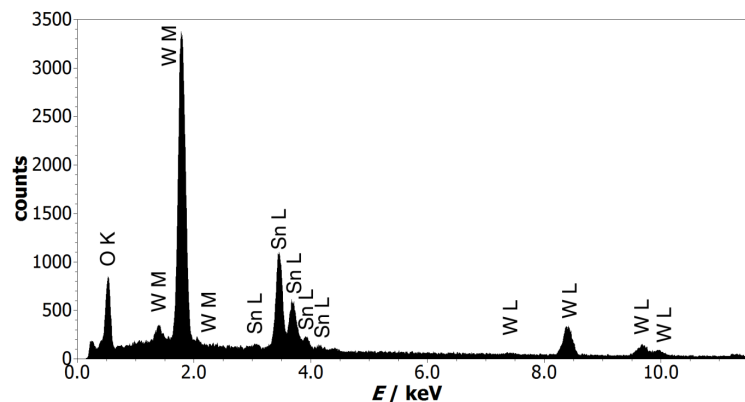


Fig. S1 EDX spectrum of faceted  $\beta$ -SnWO<sub>4</sub> microcrystals.

The surface capping of the faceted  $\beta$ -SnWO<sub>4</sub> microcrystals (title compound, sample **i**) was examined by FT-IR spectroscopy. As shown in Figure S2, a set of vibrations below 1000 cm<sup>-1</sup> is characteristic for the tungstate unit (*i.e.*, 952, 867, 813, 782 and 607 cm<sup>-1</sup>). C–H vibrations at 2918 and 2850 cm<sup>-1</sup> indicate the presence of minor amounts of organic stabilizers and solvents (*e.g.*, CTAB, DEG, ethanol) remaining on the particles surface. In fact, such organic residues might decrease the catalytic activity of the faceted  $\beta$ -SnWO<sub>4</sub> microcrystals at the beginning of the photocatalytic degradation. A certain surface capping – at least by the solvent – will however always be present on the surface of a photocatalyst that was prepared via liquid-phase methods. The very broad vibrational band centred at 3040 cm<sup>-1</sup> is finally attributed to  $\nu$ (O–H).

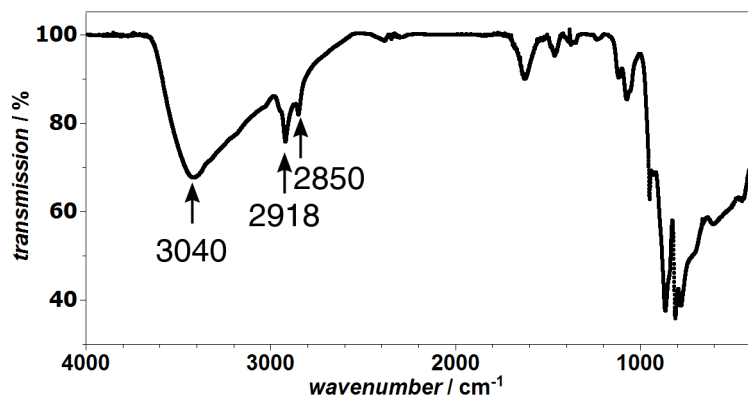
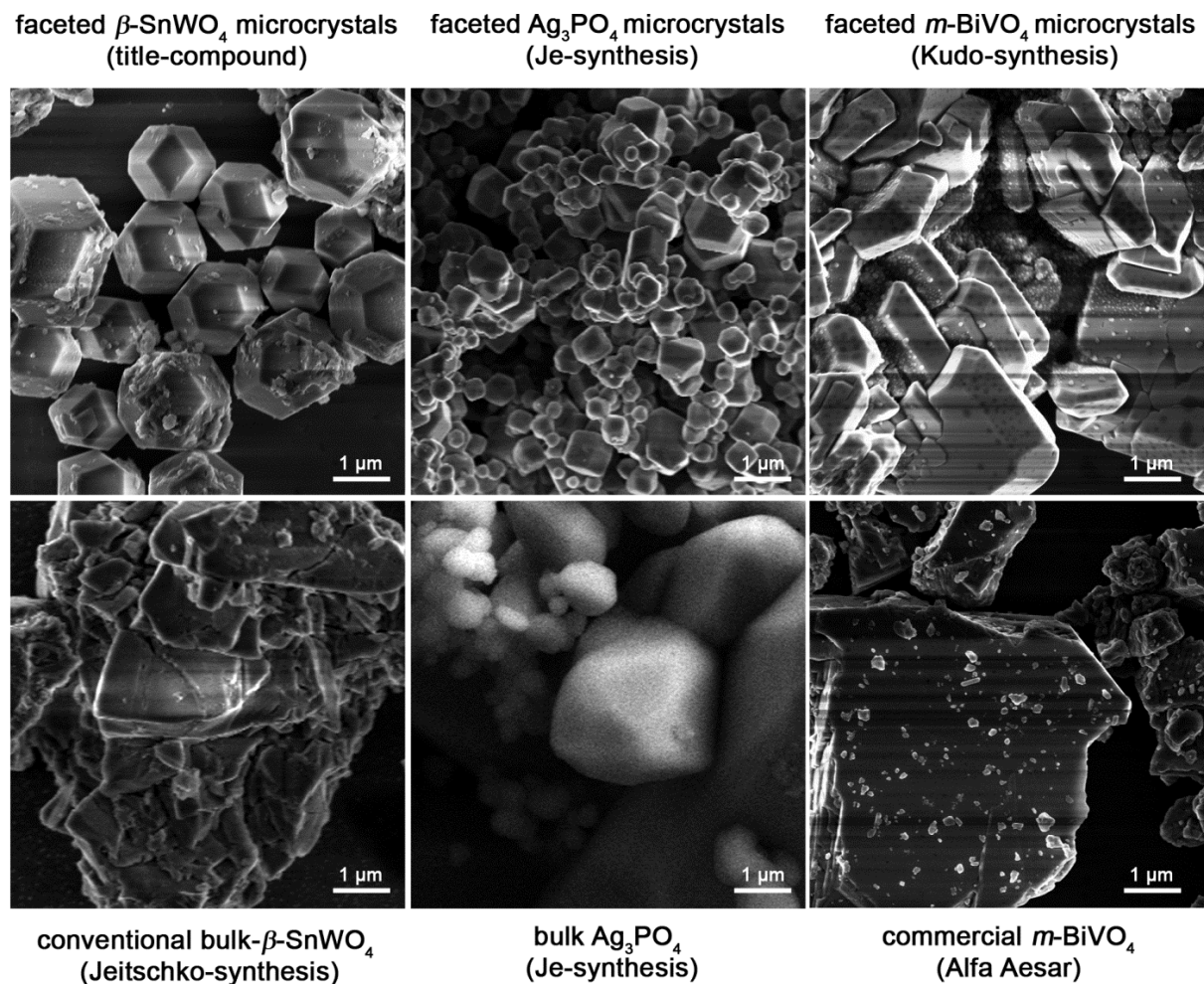


Fig. S2 FT-IR spectrum of faceted  $\beta$ -SnWO<sub>4</sub> microcrystals (title compound).

To compare size and morphology of all relevant faceted or bulk photocatalysts, Figure S3 shows low magnification SEM-images of the faceted  $\beta$ -SnWO<sub>4</sub> microcrystals (title compound, sample **i**) and of the synthesized faceted reference photocatalysts as well as of the corresponding bulk materials. This includes conventional bulk- $\beta$ -SnWO<sub>4</sub> (Jeitschko-synthesis, sample **c**), faceted Ag<sub>3</sub>PO<sub>4</sub> microcrystals (Je-synthesis, sample **g**), bulk-Ag<sub>3</sub>PO<sub>4</sub> (Je-synthesis, sample **f**), faceted BiVO<sub>4</sub> microcrystals (Kudo-synthesis, sample **d**), and commercial BiVO<sub>4</sub> microcrystals (Alfa Aesar, sample **b**).



**Fig. S3** Low magnification SEM images of the as-prepared, faceted microcrystals of  $\beta$ -SnWO<sub>4</sub> as well as of faceted and bulk Ag<sub>3</sub>PO<sub>4</sub> and *m*-BiVO<sub>4</sub> as reference photocatalysts.

To validate composition and purity, Figure S4 shows the X-ray diffraction patterns of X-ray amorphous nanoscaled  $\beta$ -SnWO<sub>4</sub> (sample **h**) and faceted  $\beta$ -SnWO<sub>4</sub>-microcrystals (title compound, sample **i**) in comparison to conventionally prepared bulk- $\beta$ -SnWO<sub>4</sub> (sample **c**). Moreover, composition and purity of the reference photocatalysts are verified. Thus, Figure S5 shows the X-ray diffraction patterns of faceted *m*-BiVO<sub>4</sub> microcrystals (sample **d**) in comparison to commercially available bulk-*m*-BiVO<sub>4</sub> (sample **b**). Figure S6 shows the X-ray diffraction patterns of faceted Ag<sub>3</sub>PO<sub>4</sub> microcrystals (sample **g**) in comparison to bulk-Ag<sub>3</sub>PO<sub>4</sub> (sample **f**).

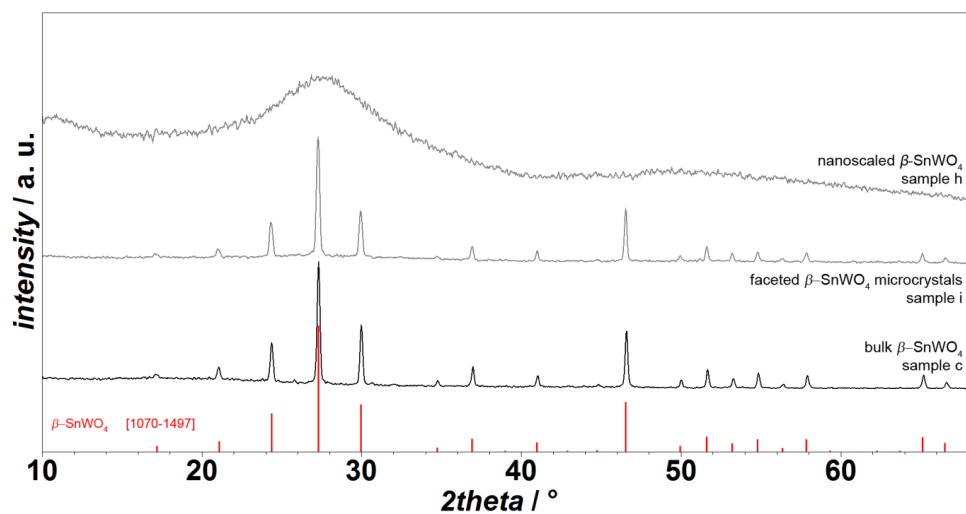


Fig. S4. XRD pattern of X-ray amorphous nanoscaled  $\beta$ -SnWO<sub>4</sub> (sample **h**), faceted  $\beta$ -SnWO<sub>4</sub> microcrystals (sample **i**), and conventionally prepared bulk- $\beta$ -SnWO<sub>4</sub> (sample **c**).

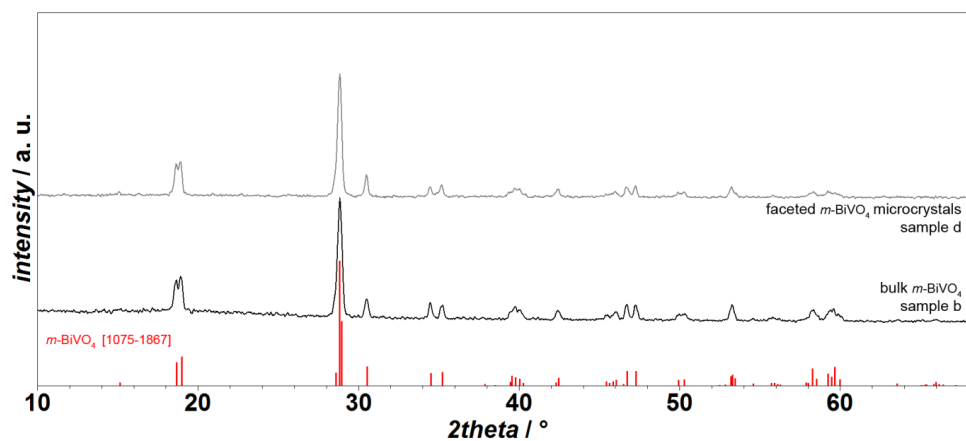


Fig. S5 XRD pattern of faceted *m*-BiVO<sub>4</sub>-microcrystals (sample **d**) and of commercially available bulk-*m*-BiVO<sub>4</sub> (sample **b**).

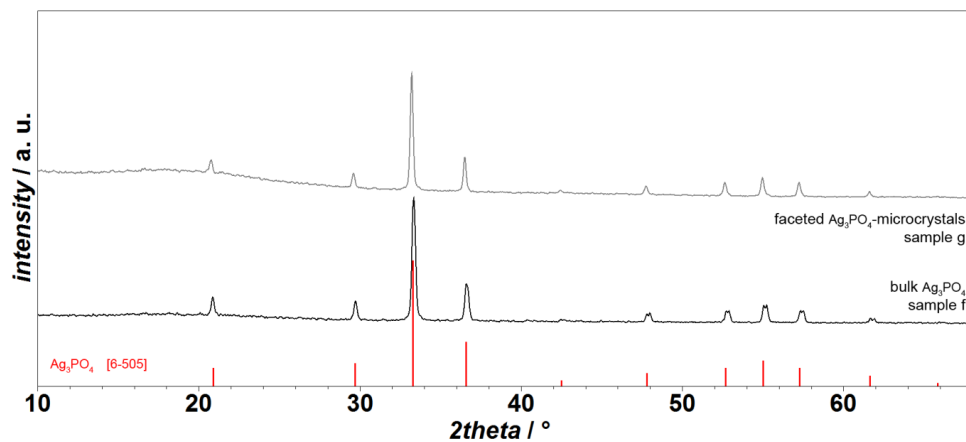


Fig. S6 XRD pattern of faceted Ag<sub>3</sub>PO<sub>4</sub> microcrystals (sample **g**), and of bulk-Ag<sub>3</sub>PO<sub>4</sub> (sample **f**).

Composition and crystallinity of the most active photocatalysts – faceted  $\beta$ - $\text{SnWO}_4$  microcrystals (sample **i**) and bulk- $\text{Ag}_3\text{PO}_4$  (sample **f**) were furthermore examined by X-ray diffraction patterns before and after the MB degradation reaction (Fig. S7). The XRD patterns that were measured after the degradation reactions, both, exhibit a relatively high background noise. This is ascribed to a certain surface contamination of intermediates and degradation products. As shown in Figure S7A, faceted  $\beta$ - $\text{SnWO}_4$  microcrystals (sample **i**) remain intact during the MB degradation reaction. In contrast, bulk- $\text{Ag}_3\text{PO}_4$  (sample **f**) clearly shows significant photocorrosion. The tendency of self-decomposition of  $\text{Ag}_3\text{PO}_4$  (sample **f**) becomes obvious by the formation of elemental silver (marked with arrows in Fig. S7B), formed from the sacrificial electron acceptor  $\text{AgNO}_3$  or from  $\text{Ag}_3\text{PO}_4$  itself, already during the first run.

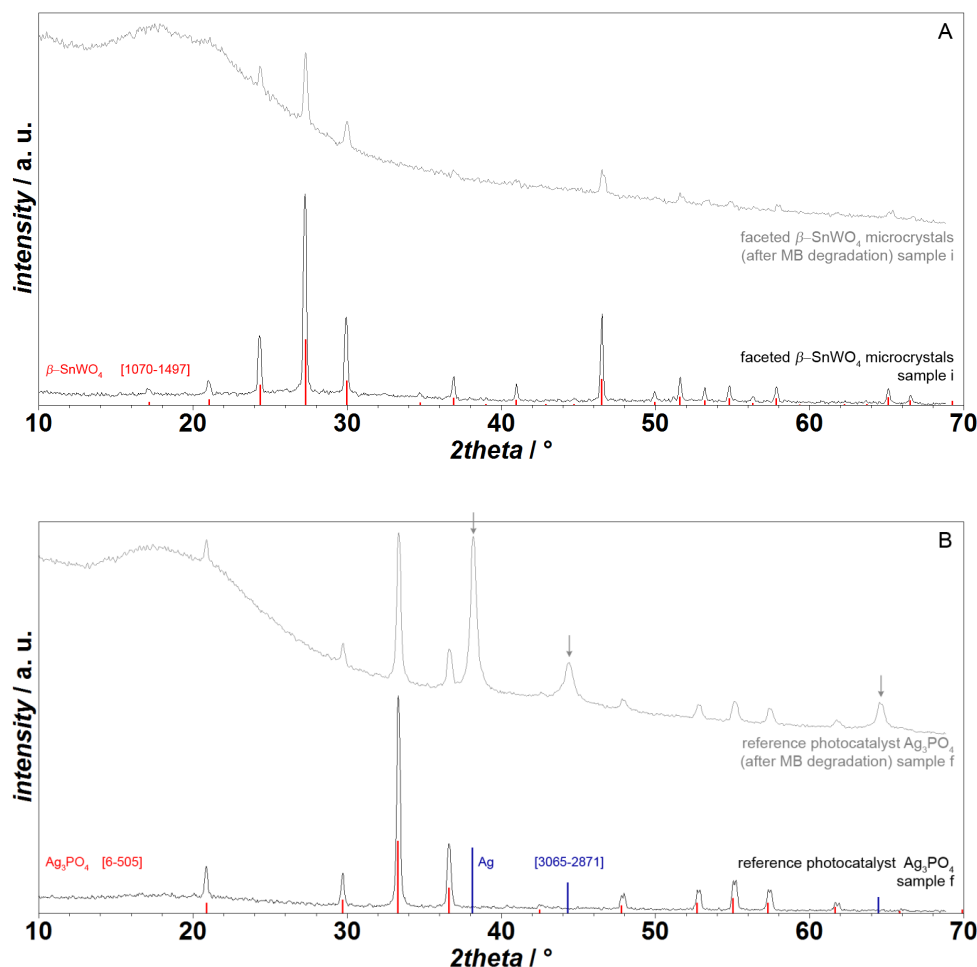
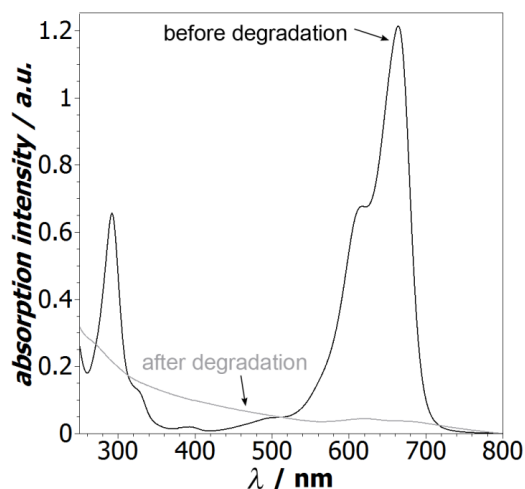


Fig. S7. (A) XRD pattern of the faceted  $\beta$ - $\text{SnWO}_4$  microcrystals (sample **i**) before and after the MB degradation reaction; (B) XRD pattern of reference photocatalyst  $\text{Ag}_3\text{PO}_4$  (sample **f**) before and after the MB degradation showing significant photocorrosion even during the first run (diffraction peaks of elemental silver indicated by arrows).

In addition, Figure S8 shows the variation of the absorption intensity of the MB dye before and after the photocatalytic degradation reaction over faceted  $\beta$ - $\text{SnWO}_4$  microcrystals (sample **i**). The apparent, non-specific increase at low wavelengths is caused by scattering of residual photocatalyst powder.



**Fig. S8.** The absorption variation of the MB dye before and after the photocatalytic degradation reaction over faceted  $\beta$ -SnWO<sub>4</sub> microcrystals (sample i).

The optical properties of the title compound as well as of the reference materials were investigated by UV-Vis spectra. Thus, Figure S9A displays the absorbance spectra of the tested photocatalysts that were derived from the diffuse reflectance spectra according to the Kubelka-Munk equation. The optical band gaps were determined from tauc-plots (Fig. S9B): The linear region in  $(ah\nu)^2$  versus  $h\nu$  plots were fitted for  $m$ -BiVO<sub>4</sub>, Ag<sub>3</sub>PO<sub>4</sub> and  $\beta$ -SnWO<sub>4</sub> samples, all exhibiting a direct band gap, whereas the best linear fit of  $(ah\nu)^{1/2}$  versus  $h\nu$  plot was taken for the determination of the band gap of Degussa P25 (sample e), which is of indirect type. The found value of 3.1 eV for the band gap of Degussa P25 (80% anatase, 20% rutile) lies between the values of pure anatase (3.2 eV) and pure rutile (3.0 eV). All found values for the optical band gaps are in good agreement with previously reported values.

Conventionally prepared bulk- $\beta$ -SnWO<sub>4</sub> (sample c) appeared greyish black as-prepared, but was of dirty yellow colour after being pestled (Fig. S10). Black and white colours have been reported for conventionally prepared bulk- $\beta$ -SnWO<sub>4</sub> before and were attributed to lattice defects.<sup>[1]</sup> Accordingly, bulk- $\beta$ -SnWO<sub>4</sub> exhibited defect absorption throughout the whole visible spectral range in addition to its band-gap absorption (*cf.* Fig S9A). A similar behaviour has been reported for TiO<sub>2</sub> appearing black due to surface defects.<sup>[5]</sup> Note that both, the XRD patterns (*cf.* Fig. S4) as well as the band-gap absorption of faceted  $\beta$ -SnWO<sub>4</sub> microcrystals (sample i) and bulk- $\beta$ -SnWO<sub>4</sub> (sample c) were found to be quite similar.

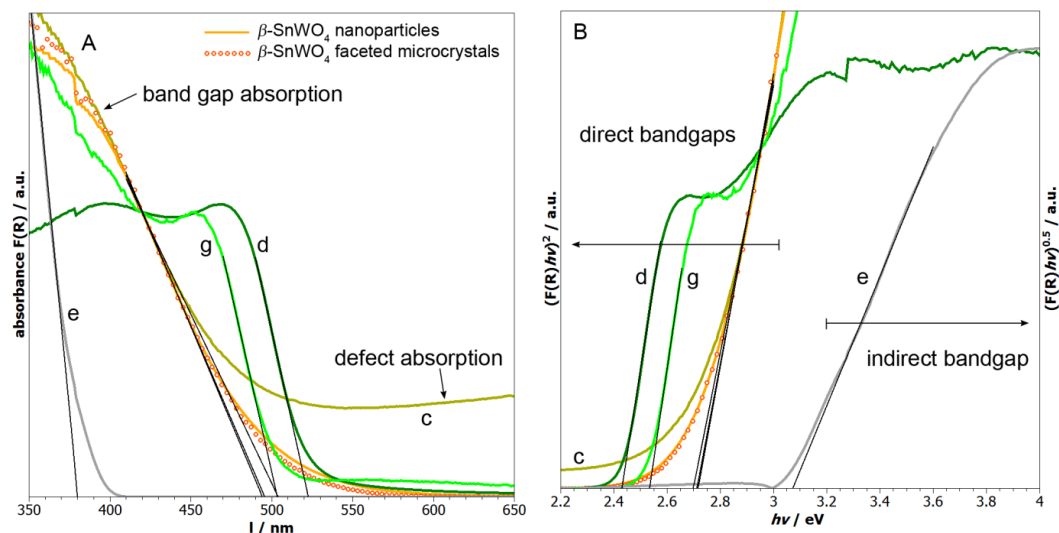


**Fig. S9.** (A) UV-Vis diffuse reflectance spectra of the as-obtained photocatalysts; (B) Tauc plots for optical band gap determination (sample c: conventionally prepared bulk- $\beta\text{-SnWO}_4$ ; sample d: faceted  $m\text{-BiVO}_4$  microcrystals; sample e: Degussa P25; sample g: faceted  $\text{Ag}_3\text{PO}_4$  microcrystals; sample h:  $\beta\text{-SnWO}_4$  nanoparticles; sample i: faceted  $\beta\text{-SnWO}_4$  microcrystals).

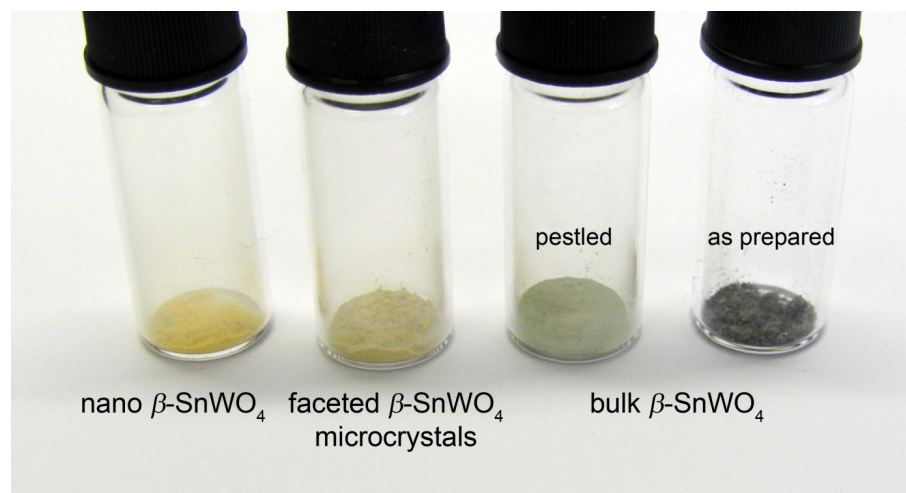


**Fig. S10.** Photographs of the as-prepared  $\beta\text{-SnWO}_4$  photocatalysts.

#### 4. Photocatalytic activity tests

The photocatalytic activity was evaluated by the oxidative decomposition of methylene blue (MB) as the most widely used model substance under simulated daylight using an Osram Xenophot HLX 64634 halogen bulb (3300 K) as the light source. For all studies, the pH of the sample was adjusted to pH 7.0. The degradation rate of the MB dye was monitored by recording the variations of the absorption-band maximum at  $\lambda_{\text{max}}$ : 664 nm in the absorbance spectrum using a Varian Cary 100 spectrometer. For continuous *in-situ* measurements, a flow-through cuvette driven by a peristaltic pump was used (Fig. S11).

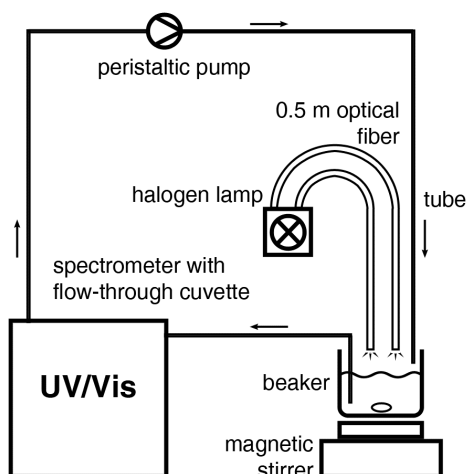


Fig. S11. Experimental set-up for the photocatalytic activity tests.

In addition to faceted  $\beta$ - $\text{SnWO}_4$  microcrystals,  $\beta$ - $\text{SnWO}_4$  nanoparticles and several benchmark photocatalysts as already presented in the main publication, further photocatalysts were tested for reasons of comparison, in addition. The benchmark photocatalysts were either reproduced from the literature (conventional bulk- $\beta$ - $\text{SnWO}_4$ ,<sup>[1]</sup> faceted  $m$ - $\text{BiVO}_4$  microcrystals;<sup>[2]</sup> faceted  $\text{Ag}_3\text{PO}_4$  rhombic dodecahedrons;<sup>[3]</sup> bulk  $\text{Ag}_3\text{PO}_4$ <sup>[4]</sup>) or were commercially available ( $\text{TiO}_2$ : Degussa P25, 80% anatase, 20% rutile, particle diameter: 25–30 nm with strong agglomeration; bulk- $m$ - $\text{BiVO}_4$ : Alfa Aesar, powder of irregular formed bulk-crystals). Note that faceted rhombic dodecahedrons of  $\text{Ag}_3\text{PO}_4$ , as used here, were reported to be the best performing available  $\text{Ag}_3\text{PO}_4$  samples, being superior to other shapes of  $\text{Ag}_3\text{PO}_4$  as for example faceted  $\text{Ag}_3\text{PO}_4$ -cubes.<sup>[3]</sup> Note that to all  $\text{Ag}_3\text{PO}_4$  samples, an equal mass of 13.1 mg  $\text{AgNO}_3$  was added as sacrificial electron acceptor as described in the original publication to exploit its full performance.<sup>[4]</sup> Apart from that, all measurements were performed under equal conditions using equimolar amounts of photocatalysts:  $c = 1.25 \cdot 10^{-3}$  M.

For measurement, all suspensions (25 mL,  $c(\text{MB}) = 2 \cdot 10^{-5}$  M) were placed in a beaker, continuously stirred magnetically and illuminated (Fig. S11). The used concentration ratios were chosen much stricter than in recent publications,<sup>[3,4,6]</sup> which were based on much higher ratios of photocatalyst to model compound. The concentrations applied here, however, follow recent prominent recommendations for comparative photocatalytic measurements,<sup>[7]</sup> and match recommended ranges as outlined in representative publications.<sup>[8]</sup> At any time, about 60 vol-% of every batch were illuminated directly while the remaining portion of the suspension was being pumped through the tube and the cuvette for measurement. In each experiment a suspension of equal catalyst concentration not being loaded with a dye was measured under equal conditions for reasons of calibration. Care has to be taken that the powders are thoroughly washed. Otherwise, MB might be *reduced* by residual traces of  $\text{Sn}^{2+}$  ions, yielding a colourless leuco-form which might be falsely interpreted as a fast oxidative decomposition. Nevertheless, these reactions can be distinguished from one another as any bleaching by reduction is much faster and reversible in contrast to the irreversible bleaching by oxidative degradation. Furthermore, the reduction

consumes  $\text{Sn}^{2+}$  whereas the oxidation is driven only by a recyclable catalyst. We already conducted recycling studies as well as tests on other organic dyes earlier.<sup>[9]</sup> Note that the presence of leuco-forms has been only barely addressed in current literature although MB represents the most often applied dye in photocatalytic degradation studies. Further details were described elsewhere.<sup>[9]</sup> Since MB has also been used in recent prominent publications<sup>[4,6]</sup> on the materials that we used as benchmark photocatalyst here, we used MB as model compound, too.

## 5. Analysis of reaction-rate constants

Figure S12 shows  $\ln(C_0/C)$  plots that were used for the determination of the reaction-rate constants  $k$  (Tab. 1). The linear relations indicate that the degradation reactions follow pseudo-first-order kinetics. In addition to the benchmark photocatalysts that are presented in the main publication (including faceted microcrystals of  $m\text{-BiVO}_4$  (sample **d**) and  $\text{Ag}_3\text{PO}_4$  (sample **g**) as well as conventionally prepared bulk- $\beta\text{-SnWO}_4$  (sample **c**), further photocatalysts were tested for reasons of comparison. These additional reference photocatalysts comprise: commercially available bulk- $m\text{-BiVO}_4$  (sample **b**), commercially available  $\text{TiO}_2$  (sample **e**, Degussa P25) as the most studied photocatalyst and bulk- $\text{Ag}_3\text{PO}_4$  (sample **f**).

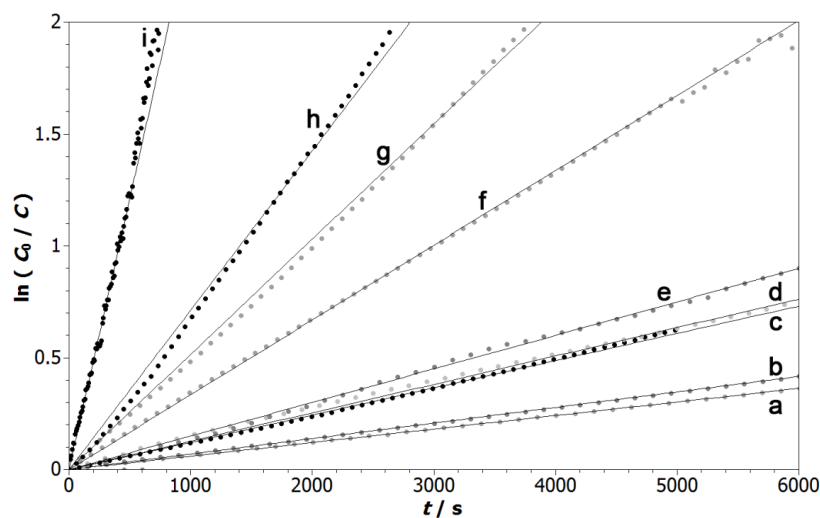


**Fig. S12.**  $\ln(C_0/C)$  plots for the determination of the rate constants  $k$  with sample **a**: photolysis; sample **b**: commercial  $m\text{-BiVO}_4$ ; sample **c**: bulk- $\beta\text{-SnWO}_4$ ; sample **d**: faceted  $m\text{-BiVO}_4$  microcrystals; sample **e**: Degussa P25; sample **f**: bulk- $\text{Ag}_3\text{PO}_4$ ; sample **g**: faceted  $\text{Ag}_3\text{PO}_4$  microcrystals; sample **h**:  $\beta\text{-SnWO}_4$  nanoparticles; sample **i**: faceted  $\beta\text{-SnWO}_4$  microcrystals (title compound).

**Tab. 1.** Comparison of faceted  $\beta$ -SnWO<sub>4</sub> microcrystals (title compound, sample **i**) and high-surface  $\beta$ -SnWO<sub>4</sub> nanoparticles (sample **h**) with state-of-the-art photocatalysts as reference materials.

sample		BET / m <sup>2</sup> g <sup>-1</sup>	E <sub>G</sub> / eV	k / s
<b>a</b>	photolysis	no catalyst		6.0 · 10 <sup>-5</sup>
<b>b</b>	<i>m</i> -BiVO <sub>4</sub>	bulk	2.43	7.0 · 10 <sup>-5</sup>
<b>c</b>	$\beta$ -SnWO <sub>4</sub>	bulk	2.70	1.2 · 10 <sup>-4</sup>
<b>d</b>	<i>m</i> -BiVO <sub>4</sub>	faceted microcrystals	2.43	1.3 · 10 <sup>-4</sup>
<b>e</b>	TiO <sub>2</sub> (Degussa P25)	nanoparticles	3.07	1.5 · 10 <sup>-4</sup>
<b>f</b>	Ag <sub>3</sub> PO <sub>4</sub>	bulk	2.47	3.3 · 10 <sup>-4</sup>
<b>g</b>	Ag <sub>3</sub> PO <sub>4</sub>	faceted microcrystals	2.53	5.2 · 10 <sup>-4</sup>
<b>h</b>	$\beta$ -SnWO <sub>4</sub>	nanoparticles	2.71	7.1 · 10 <sup>-4</sup>
<b>i</b>	$\beta$ -SnWO <sub>4</sub>	faceted microcrystals	2.72	2.4 · 10 <sup>-3</sup>

## Notes and references

- 1 W. Jeitschko and A. W. Sleight, *Acta Cryst. B*, 1972, **28**, 3174.
- 2 a) A. Kudo, K. Omori and H. Kato, *J. Am. Chem. Soc.*, 1999, **121**, 11459; b) S. Kohtani, S. Makino, A. Kudo, K. Tokumura, Y. Ishigaki, T. Matsunaga, O. Nikaido, K. Hayakawa and R. Nakagaki, *Chem. Lett.*, 2002, **31**, 2002.
- 3 Y. Bi, S. Ouyang, N. Umezawa, J. Cao and J. Ye, *J. Am. Chem. Soc.*, 2011, **133**, 6490.
- 4 Z. Yi, J. Ye, N. Kikugawa, T. Kako, S. Ouyang, H. Stuart-Williams, H. Yang, J. Cao, W. Luo, Z. Li, Y. Liu and, R. L. Withers, *Nat. Mater.*, 2010, **9**, 559.
- 5 X. Chen, L. Liu, P. Y. Yu and S. S. Mao, *Science*, 2011, **331**, 746.
- 6 Y. Bi, H. Hu, S. Ouyang, G. Lu, J. Cao and J. Ye, *Chem. Commun.*, 2012, **48**, 3748.
- 7 T. Maschmeyer and M. Che, *Angew. Chem. Int. Edit.*, 2010, **49**, 9590.
- 8 a) Y. Zhou, K. Vuille, A. Heel, B. Probst, R. Kontic and G. R. Patzke, *Appl. Catal. A*, 2010, **375**, 140; b) S. Lakshmi, R. Renganathan and S. Fujita, *J. Photochem. Photobiol. A*, 1995, **88**, 163; c) G. Sivalingam, K. Nagaveni, M. S. Hegde and G. Madras, *Appl. Catal. B*, 2003, **45**, 23; d) N. Guettaï and H. A. Amar, *Desalination*, 2005, **185**, 439.
- 9 J. Ungelenk and C. Feldmann, *Appl. Catal. B*, 2011, **102**, 515.